Bone Reports 3 (2015) 83–94

Contents lists available at ScienceDirect

Bone Reports

journal homepage: www.elsevier.com/locate/bonr

Massive elimination of multinucleated osteoclasts by eupatilin is due to dual inhibition of transcription and cytoskeletal rearrangement

Ju-Young Kim [a,1], Myeung Su Lee [a,b,c,1], Jong Min Baek [d,1], Jongtae Park [e], Byung-Soo Youn [f,g,*], Jaemin Oh [a,b,c,d,**]

[a] Imaging Science-based Lung and Bone Diseases Research Center, Wonkwang University, Iksan, Jeonbuk 570-749, Republic of Korea
[b] Division of Rheumatology, Department of Internal Medicine, Wonkwang University, Iksan, Jeonbuk 570-749, Republic of Korea
[c] Institute for Skeletal Disease, Wonkwang University, Iksan, Jeonbuk 570-749, Republic of Korea
[d] Department of Anatomy, School of Medicine, Wonkwang University, Iksan, Jeonbuk 570-749, Republic of Korea
[e] Department of Neurosurgery, Wonkwang University, Iksan, Jeonbuk 570-749, Republic of Korea
[f] Biomedical Research Center, University of Ulsan College of Medicine, Ulsan University Hospital, 877 Bangeojinsunwhando-ro, Dong-Ku, Ulsan 682-714, Republic of Korea
[g] OsteoNeuroGen 40 MiKeum-ro, Bundang, Kyunggi 461-871, Republic of Korea

ARTICLE INFO

Article history:
Received 30 June 2015
Received in revised form 16 September 2015
Accepted 4 October 2015
Available online 8 October 2015

Keywords:
Osteoclastogenesis;
Transcriptional repression;
Actin depolymerization;
Cytoskeletal rearrangement

ABSTRACT

Osteoporosis is an aging-associated disease requiring better therapeutic modality. Eupatilin is a major flavonoid from *Artemisia* plants such as *Artemisia princeps* and *Artemisia argyi* which has been reported to possess various beneficial biological effects including anti-inflammation, anti-tumor, anti-cancer, anti-allergy, and anti-oxidation activity. Complete blockade of RANK-dependent osteoclastogenesis was accomplished upon stimulation prior to the receptor activator of nuclear factor κB (RANK)-ligand (RANKL) treatment or post-stimulation of bone marrow macrophages (BMCs) in the presence of RANKL with eupatilin. This blockade was accompanied by inhibition of rapid phosphorylation of Akt, GSK3β, ERK and IκB as well as downregulation of c-Fos and NFATc1 at protein, suggesting that transcriptional suppression is a key mechanism for anti-osteoclastogenesis. Transient reporter assays or gain of function assays confirmed that eupatilin was a potent transcriptional inhibitor in osteoclasts (OC). Surprisingly, when mature osteoclasts were cultured on bone scaffolds in the presence of eupatilin, bone resorption activity was also completely blocked by dismantling the actin rings, suggesting that another major acting site of eupatilin is cytoskeletal rearrangement. The eupatilin-treated mature osteoclasts revealed a shrunken cytoplasm and accumulation of multi-nuclei, eventually becoming fibroblast-like cells. No apoptosis occurred. Inhibition of phosphorylation of cofilin by eupatilin suggests that actin may play an important role in the morphological change of multinucleated cells (MNCs). Human OC similarly responded to eupatilin. However, eupatilin has no effects on osteoblast differentiation and shows cytotoxicity on osteoblast in the concentration of 50 μM. When eupatilin was administered to LPS-induced osteoporotic mice after manifestation of osteoporosis, it prevented bone loss. Ovariectomized (OVX) mice remarkably exhibited bone protection effects. Taken together, eupatilin is an effective versatile therapeutic intervention for osteoporosis via; 1) transcriptional suppression of c-Fos and NFATc1 of differentiating OC and 2) inhibition of actin rearrangement of pathogenic MNCs.

Abbreviations: OB, osteoblasts; OC, osteoclasts; HDACis, Histone deacetylase inhibitors; RANK, the receptor activator of nuclear factor κB; RANKL, RANK ligand; M-CSF, macrophage colony-stimulating factor; SOST, sclerostin; FBS, fetal bovine serum; α-MEM, α-minimum essential medium; MNCs, multinucleated cells; NFATc1, nuclear factor of activated T cells c1; BMCs, bone marrow cells; BMMs, bone marrow macrophages; TRAP, tartrate-resistant acid phosphate; XTT, sodium3'-[1-(phenyl-aminocarbonyl)-3,4-tetrazolium]-bis(4-methoxy-6-nitro); PGE_2, prostaglandin E_2; TBST, tris-buffered saline contacting 0.1% Tween-20; ALP, alkaline phosphatase; LPS, lipopolysaccharide; OVX, ovariectomized; μCT, micro-computed tomography; H&E, hematoxylin and eosin; SD, standard deviation; SE, standard error.

* Correspondence to: B.-S, Youn, Biomedical Research Center, University of Ulsan College of Medicine, Ulsan University Hospital, 877 Bangeojinsunwhando-ro, Dong-Ku, Ulsan 682-714, Republic of Korea.
** Correspondence to: J. Oh, Department of Anatomy, School of Medicine, Wonkwang University, Iksan, Jeonbuk 570-749, Republic of Korea.
E-mail addresses: byung4jc@gmail.com (B.-S. Youn), jmoh@wku.ac.kr (J. Oh).
[1] These authors contributed equally to this manuscript.

http://dx.doi.org/10.1016/j.bonr.2015.10.003

1. Introduction

Osteoporosis is an aging-associated disease requiring unmet medical needs. Osteoblasts (OBs) and osteoclasts (OCs) are major players for regulated bone formation and/or bone loss as a homeostatic balance for differentiation of bone progenitor cells (Geusens et al., 2014). Uncontrolled expansion of OCs due to physiological changes such as menopause or inflammation leads to osteoporosis. In addition, in generalized bone diseases, OCs seem to be engaged in the process of bone tumor metastasis (Suda et al., 1999). Currently, bisphosphonate-derivatives or calcitonin are major therapeutics but have apparent disadvantages such as non-metabolized matter. Although receptor activator of nuclear factor κB (RANK)-ligand (RANKL) antibody treatment is being used and anti-sclerostin (SOST) antibody treatment may be soon available to osteoporosis, costs or their long-term safety remains to be explored given that RANKL is involved in dendritic cell function and SOST seems to be involved in Wnt signaling (Williamson et al., 2002; Semënov et al., 2005). Hence, the necessity for novel therapeutic interventions is evident for osteoporosis. Histone deacetylase inhibitors (HDACis) have exerted potent osteogenic potential related to stability of Runx2 by deacetylases (Kim et al., 2011; Jeon et al., 2006). As such there have been a great number of small molecules or natural products that have been shown to affect osteoclastogenesis (Kim et al., 2014a,b; Lee et al., 2014; Kwak et al., 2010). Although the RANKL/RANK axis is the master regulator for osteoclastogenesis, precise underlying mechanisms for contribution of many coupling factors such as SOST, semaphorin, OSCAR, FcR or OC-STAMP to osteoclastogenesis remains to be explored (Honma et al., 2014). In particular, the formation of an actin ring, which is the hallmark of OC function or bone resorption mechanism has not fully appreciated. Therefore, it is possible that there exists a myriad of small molecules affecting osteoclastogenesis acting on this wide range of coupling factors, thereby dampening down formation of multinucleated cells (MNCs) or bone resorption. The RANK/RANKL axis is the master regulator for formation of TRAP + OCs (Takayanagi et al., 2002). Development of a versatile therapeutic intervention via combinatorial blockade for both the early differentiation process and later bone resorption of OCs could create a powerful therapeutic modality. Artemisia has been safely used for many inflammatory diseases as herbal extracts for a few thousand years (van der Kooy and Sullivan, 2013; Cha et al., 2009; Choi et al., 2011; Kim et al., 2009; Ho et al., 2014). Eupatilin is an O-methylated flavonoid (Son et al., 2013). A great number of flavonoids have anti-oxidant potential or apoptotic effects on tumor cells (Ji et al., 2014). Although several flavonoids except some species have been demonstrated to have osteogenic capabilities, underlying molecular mechanisms remain to be largely unexplored (Yamaguchi et al., 2007). Also, a recent report demonstrated the anti-arthritic effect of eupatilin on collagen-induced arthritis (CIA) mice model (Kim et al., 2015). However, the relationship between eupatilin and osteoporotic mice model has not been explored.

Here, we show that eupatilin is a potent inhibitor of the formation of MNCs in vitro via both the suppression of key transcription factors and polymerization actin ring formation. As such, the in vivo administration of eupatilin into mice substantially prevented the onset of bone loss caused by ovariectomy or inflammation. Eupatilin was also able to completely block formation of human MNCs in vitro.

2. Materials and methods

2.1. Mice and reagents

Male, 5-week-old ICR mice were purchased from Damul Science (Daejeon, Korea). Ten-week-old OVX mice were purchased from Central Lab. Animal Inc. (Seoul, Korea). Mice were kept in a temperature (22 °C–24 °C) and humidity (55%–60%) controlled environment with a 12 h light/dark cycle. All experiments were performed in accordance with guidelines for animal experimentation of the Institute Committee of Wonkwang University. Eupatilin was obtained from DONG-A PHARM (Seoul, Korea). Soluble, recombinant human M-CSF and human RANKL were obtained from PeproTech EC, Ltd. (London, UK). Anti-Akt, anti-phospho-Akt, anti-GSK3β, anti-phospho-GSK3β, anti-IκB, anti-phospho-IκB, anti-Cofilin, anti-phospho-Cofilin, anti-p38, anti-phospho-p38, anti-ERK, anti-phospho-ERK, anti-JNK, and anti-phospho-JNK antibodies were purchased from Cell Signaling Technology, Inc. (Beverly, MA, USA). Anti-c-Fos, and anti-NFATc1 antibodies were purchased from Santa Cruz Biotechnology (Santa Cruz, CA, USA). A monoclonal β-actin antibody was obtained from Sigma (St. Louis, MO, USA). Fetal bovine serum (FBS), α-minimum essential medium (α-MEM), and penicillin/streptomycin were purchased from Gibco BRL (Grand Island, NY, USA). All other chemicals were of analytical grade or complied with the standards required for cell culture.

2.2. Human and mouse bone marrow macrophage preparation

Human bone marrow cells (BMCs) were obtained from healthy volunteers and were separated by density gradient centrifugation using Ficoll–Histopaque (Sigma-Aldrich, St. Louis, MO, USA). These cells were cultured for 7 days in the presence of M-CSF (100 ng/mL). Mouse BMCs obtained from 10-week-old C57BL/6J female mice by flushing the femurs and tibias were seeded on culture dishes in α-MEM supplemented with 10% FBS and M-CSF (10 ng/mL). Non-adherent cells were transferred to 10-cm petri dishes and cultured in the presence of M-CSF (30 ng/mL) for an additional 3 days.

2.3. In vitro osteoclastogenesis assay

BMCs were obtained from 5-week-old male ICR mice by flushing femurs and tibias with α-MEM supplemented with 10% FBS, penicillin (100 U/mL), and streptomycin (100 μg/mL) and from human bone marrow. To obtain BMMs, BMCs were seeded on culture dishes in α-MEM supplemented with 10% FBS and M-CSF (10 ng/mL) and cultured for 1 day. Non-adherent cells were transferred to 10-cm petri dishes and further cultured in the presence of M-CSF (30 ng/mL) for 3 days. After non-adherent cells were removed, adherent cells were used as BMCs, which contain osteoclast precursors. To generate osteoclasts from these BMCs, cells were seeded in a 48-well plate (3.5×10^4 cells/well) in complete medium containing M-CSF (30 ng/mL) and RANKL (100 ng/mL) and cultured for 4 days with or without eupatilin. The cells were fixed in 3.7% formalin for 10 min, permeabilized with 0.1% Triton X-100, and then stained with TRAP (Sigma). TRAP-positive MNCs with more than three nuclei were counted as osteoclasts.

2.4. Pre-treatment with eupatilin in osteoclastogenesis assay

Bone marrow macrophages (BMMs) were cultured in the presence only of M-CSF (10 ng/mL) for 1 day. After pre-treatment of BMMs with eupatilin for the indicated times, the cells were cultured in a new medium containing M-CSF (30 ng/mL) and RANKL (100 ng/mL) for 3 or 4 days. The cells were stained with a TRAP solution as described above. TRAP-positive osteoclasts with more than five nuclei and multinucleated cells with more than three nuclei were counted as osteoclasts.

2.5. Post-treatment with eupatilin in osteoclastogenesis assay

BMMs were cultured in the presence of M-CSF (30 ng/mL) and RANKL (100 ng/mL) for 3 days. Before TRAP staining, BMMs were post-treated with eupatilin for the indicated times and then cells were stained with a TRAP solution as described above.

2.6. Cytotoxicity assay

The XTT (sodium3′-[1-(phenyl-aminocarbonyl)-3,4-tetrazolium]-bis(4-methoxy-6-nitro) assay was performed to examine the effects of eupatilin on the viability of BMCs. Mouse BMCs (1×10^4 cells/well) were seeded in 96-well plates with various concentrations of eupatilin and incubated for 3 days in the presence of M-CSF (30 ng/mL). Then, XTT solution (50 μL) was added to each well and incubated for 4 h. The plate was read at 450 nm with an ELISA reader (Molecular Devices, CA, USA) and interpolated from a standard curve.

2.7. Western blot analysis and quantitative real-time polymerase chain reaction (RT-PCR) analysis

Western blot analysis, and quantitative RT-PCR were performed as described previously (Kim et al., 2014c). We performed Western blotting by using 1:1000 dilution of primary antibodies with a source of rabbit or mouse reconstituted at 1 mg/mL and 1:3000 anti-rabbit and -mouse secondary antibodies reconstituted at 0.4 mg/mL. The expression data of quantitative RT-PCR were calculated from the cycle threshold (Ct) value using the delta–delta Ct (Livak) method by using those primer sets as shown in Table 1.

2.8. Pit formation assay

BMCs (1×10^7 cells) and primary osteoblasts (1×10^6 cells) were seeded on collagen gel-coated culture dishes and cultured for 7 days in the presence of 10^{-8} M 1,25-dihydroxyvitamin D_3 (Sigma) and 10^{-6} M prostaglandin E_2 (PGE_2) (Sigma). The co-cultured cells were detached by 0.1% collagenase treatment at 37 °C for 10 min and were then replated on hydroxyapatite-coated plates (Corning, Corning, NY, USA) for 24 h and dentin slices for 48 h. Cells attached to the plates or dentin slices were removed and the total resorption pits were photographed by microscopy and analyzed using Image-Pro Plus version 4.0 (Media Cybernetics, Silver Spring, MD, USA).

Table 1
Primer sequences for real-time RT-PCR.

TRAP	Forward: 5′-TCA TGG GTG GTG CTG CT-3′
	Reverse: 5′-GCC CAC AGC CAC AAA TCT-3′
c-Fos	Forward: 5′-GGT GAA GAC CGT GTC AGG AG-3′
	Reverse: 5′-TAT TCC GTT CCC TTC GGA TT-3′
NFATc1	Forward: 5′-GAG TAC ACC TTC CAG CAC CTT-3′
	Reverse: 5′-TAT GAT GTC GGG GAA AGA GA-3′
Cathepsin K	Forward: 5′-CCA GTG GGA GCT ATG GAA GA-3′
	Reverse: 5′-CTC CAG GTT ATG GGC AGA GA -3′
OSCAR	Forward: 5′-GGA ATG GTC CTC ATC TGC TT-3′
	Reverse: 5′-TCC AGG CAG TCT CTT CAT TTT-3′
DC-STAMP	Forward: 5′-TCC TCC ATG AAC AAA CAG TTC CA-3′
	Reverse: 5′-AGA CGT GGT TTA GGA ATG CAG CTC-3′
OC-STAMP	Forward: 5′-ATG AGG ACC ATC AGG GCA GCC ACG-3′
	Reverse: 5′-GGA GAA GCT GGG TCA GTA GTT CGT-3′
Integrin αv	Forward: 5′-ACA AGC TCA CTC CCA TCA CC-3′
	Reverse: 5′-ATA TGA GCC TGC CGA CTG AC-3′
Integrin β3	Forward: 5′-GGA GTG GCT GAT CCA GAT GT-3′
	Reverse: 5′-TCT GAC CAT CTT CCC TGT CC-3′
ICAM-1	Forward: 5′-CAT GCC TTA GCA GCT GAA CA-3′
	Reverse: 5′-AGC TTG CAC GAC CCT TCT AA-3′
TESK1	Forward: 5′-AAG AAC ACG CAT TGG CCT AC-3′
	Reverse: 5′-CGT CTT GAG AGT GCA CCG TA-3′
LIMK2	Forward: 5′-GAC CAG CTA CGG CTA GAT GC-3′
	Reverse: 5′-TCA GTG TCC CCT CCT GAT TC-3′
Cofilin	Forward: 5′-CCT CTG GTG TGG CTG TCT CT-3′
	Reverse: 5′-GCC TTC TTG CGT TTC TTC AC-3′
GAPDH	Forward: 5′-TCA AGA AGG TGG TGA AGC AG-3′
	Reverse: 5′-GGT GGA GGA GTG GGT GTC-3′

2.9. Osteoblastic cell culture and assays

To culture osteoblasts, calvarias of neonatal mice were digested with 0.1% collagenase and 0.2% dispase 5 times, and cells isolated in the last 3 digestions were combined and cultured in α-MEM containing 10% FBS, 100 U/mL penicillin, and 100 μg/mL streptomycin. To measure alkaline phosphatase (ALP) activity, primary osteoblasts were inoculated at a density of 2×10^4 cells/well and cultured in the absence or presence of 50 μg/mL ascorbic acid and 10 mM β-glycerol phosphate. On differentiation day 7, cells were sonicated in 50 mM Tris–HCl buffer (pH 7.4) containing 1% Triton X-100, 150 mM NaCl, and 1 mM EDTA. Then, 100 μL of substrate (*p*-nitrophenylphosphate) (Sigma) was added to the cells, and the plate was incubated for 30 min at 37 °C. The amount of *p*-nitrophenol released was determined by measuring absorbance at 405 nm using a microplate reader. For ALP staining, cells were fixed in 70% ethanol and stained for 10–20 min with a solution containing 0.01% naphthol, AS-MX phosphate, 1% N,N-dimethyl formamide, and 0.06% fast blue BB (Sigma).

2.10. Retrovirus preparation and infection

Retroviral vectors pMX-IRES-EGFP, pMX-cFos-IRES-EGFP, pMX-constitutively active (CA)-NFATc1-IRES-EGFP, pMX-CA-IKKβ-IRES-EGFP, and pMX-Akt-IRES-EGFP were used for transient transfection of these pMX vectors into Plat-E retroviral packaging cells using X-tremeGENE 9 (Roche, Nutley, NJ, USA) according to the manufacturer's protocol. After incubation in a fresh medium for 2 days, culture supernatants of the retrovirus-producing cells were collected. For retroviral infection, non-adherent BMCs were cultured in M-CSF (30 ng/mL) for 2 days. BMMs were incubated with viral supernatant pMX-IRES-EGFP, pMX-cFos-IRES-EGFP, pMX-CA-NFATc1-IRES-EGFP, pMX-CA-IKKβ-IRES-EGFP, and pMX-Akt-IRES-EGFP virus-producing Plat-E cells together with polybrene (10 μg/mL) and M-CSF (30 ng/mL) for 6 h. The infection efficiency of retroviruses was determined by green fluorescent protein expression, and was always greater than 80%. After infection, BMMs were induced to differentiate in the presence of M-CSF (30 ng/mL) and RANKL (100 ng/mL) for 4 days. Osteoclast formation was detected by TRAP staining.

2.11. Immunofluorescence confocal microscopy

BMMs were incubated with M-CSF (30 ng/mL) and RANKL (100 ng/mL) in the presence of DMSO or eupatilin. After 3 days, a culture medium was replaced with a fresh medium containing the same ingredient. One day later, the cells were fixed in 3.7% formalin for 20 min, permeabilized with 0.1% Triton X-100 for 15 min, incubated with 0.25% bovine serum albumin for 30 min, and stained with phalloidin and DAPI solution to visualize F-actin and nuclei, respectively (Life Technology, Seoul, Korea). Fluorescence detection of cells was observed under a laser scanning confocal microscope (Olympus FV1200, Japan). Images were analyzed by the Image-Pro Plus software (USA) and are representative of five experiments.

2.12. Mice and treatments

To study the preventive effect of eupatilin on lipopolysaccharide (LPS)-induced osteoclast formation in vivo, ICR mice were divided into 4 experimental groups comprised of 5 mice each: the phosphatebuffered saline (PBS)-treated (Control), only LPS-treated, only eupatilin-treated, and LPS and eupatilin-treated groups. Eupatilin (10 mg/kg) or PBS was administered orally 1 day before LPS injection (5 mg/kg). Eupatilin or PBS was administered orally every other day for 8 days. LPS was injected intraperitoneally on days 1 and 4. The mice were killed after 8 days, and the left femurs were analyzed by high-resolution micro-computed tomography (μ-CT). The right femurs were fixed in 4% paraformaldehyde (Sigma) for 1 day, decalcified

for 3 weeks in 12% EDTA, and then embedded in paraffin. Sections (5-μm thick) were prepared using a Leica microtome RM2145 (Leica Microsystems, Bannockburn, IL, USA), and were stained with hematoxylin and eosin (H&E). To confirm the therapeutic effect of eupatilin on LPS-induced bone loss in vivo, ICR mice were divided into 6 experimental groups comprised of 5 mice each: PBS-treated (Control), LPS-treated, and LPS plus eupatilin-treated groups. Eupatilin (10 mg/kg) or PBS was administered orally every day from 4, 6, or 8 days. LPS was injected intraperitoneally on days 1 and 4. Mice were killed after 5 days (only LPS-treated Day 5 group) or 10 days. Mice were killed after 10 days, and the left femurs were analyzed by high-resolution μ-CT. We further assessed the effect of eupatilin on ovariectomy (OVX)-induced bone loss. Eight-week-old female C57BL/6 mice were either 6 sham-operated mice or 12 OVX mice. OVX mice were divided into two groups: OVX control (PBS) and eupatilin (10 mg/kg) groups. After, eupatilin was administrated orally for 4 weeks. The μCT images, analysis of several parameters, and histological data were acquired as described above.

2.13. μCT analysis

Femur metaphysic regions were scanned using a high-resolution μCT (NFR-Polaris-S160; Nanofocus Ray, Iksan, Korea) with a source voltage of 60 kVp, current of 114 μA and 7 μm isotropic resolution. Femur scans were performed from the growth plate proximally to 2 mm, with 350 sections per scan. Bone histomorphometric analyses were performed with μCT data using INFINITT-Xelis software (INFINITT Healthcare, Seoul, Korea). Structural parameters were trabecular bone volume/total volume (BV/TV, %), trabecular thickness (Tb·Th, μm), trabecular separation (Tb·Sp, μm), and trabecular number (Tb·N, 1/mm).

2.14. Statistical analyses

Experiments were conducted at least three times, and the data are expressed as the mean ± standard deviation (SD) or the mean ± standard error (SE). All statistical analyses were performed by using the Statistical Package for the Social Sciences Software (SPSS; Korean version 14.0). Most statistical differences were analyzed using one-

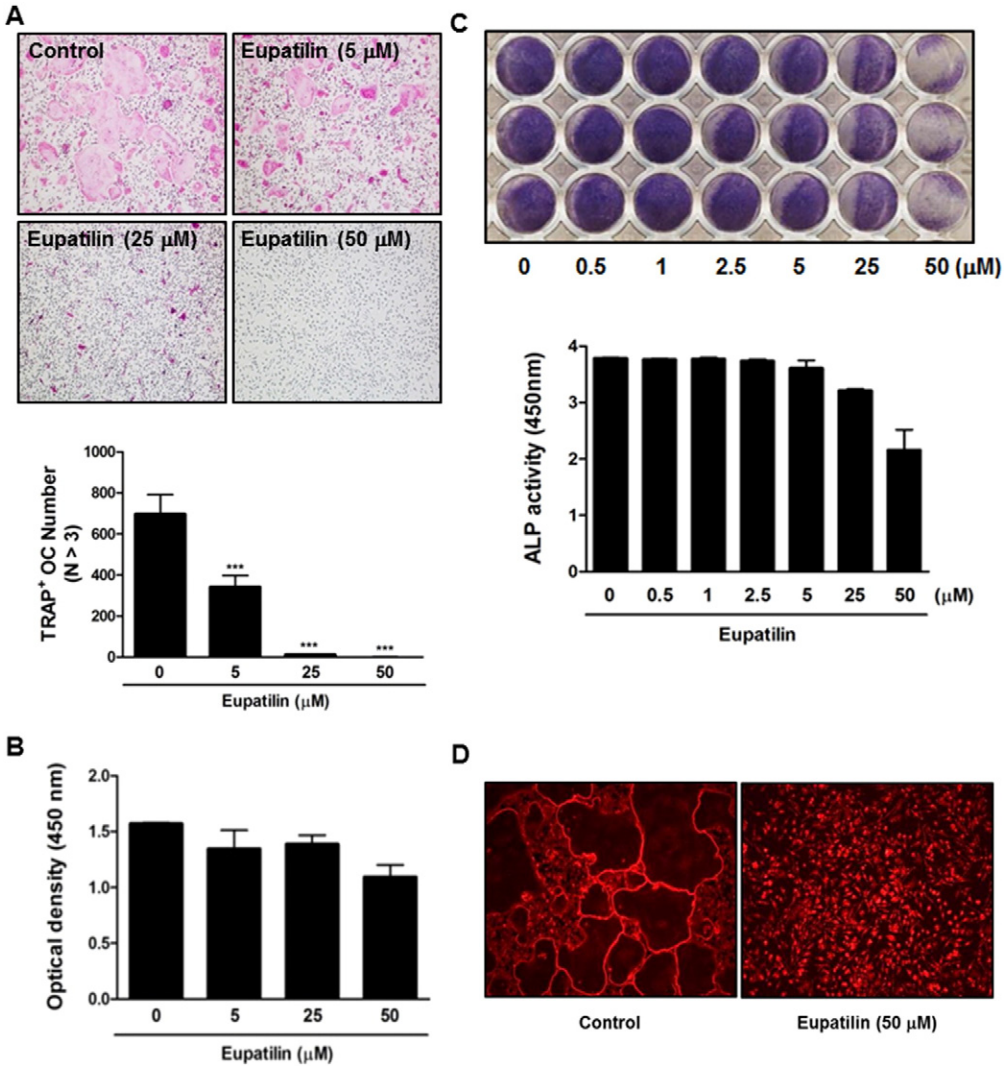

Fig. 1. Potent anti-osteoclastogenic capability of eupatilin and effects of eupatilin on cytotoxicity and osteoblasogenesis. (A) Mouse BMCs were cultured for 4 days in the presence of M-CSF (30 ng/mL) and RANKL (100 ng/mL) with control media or eupatilin. Cells were fixed and stained with TRAP solution (upper). TRAP-positive MNCs were counted as osteoclasts (lower). The magnification of images is 10×. (B) Cell viability was determined by XTT assay using BMCs. (C) Primary osteoblasts were treated with various concentrations of eupatilin for 7 days in the presence of 50 μg/mL ascorbic acid and 10 mM β-glycerol phosphate. ALP positive cells were stained with ALP solution. ***$P < 0.001$ versus the control. (D) Mouse BMCs were cultured for 4 days in the presence of M-CSF and RANKL with eupatilin (50 μM) or control (DMSO). Cells were fixed with 3.7% formalin in PBS, permeabilized with 0.1% Triton X-100 in PBS and stained with rhodamine phalloidin for actin ring. The magnification of images is 10×.

way ANOVA followed by Tukey's post hoc test. *P*-values of less than 0.05 were considered statistically significant.

3. Results

3.1. Eupatilin is a potent inhibitor of NFATc1 transcription

To see if eupatilin exerts effects on bone homeostasis we stimulated mouse BMCs with various concentrations of eupatilin in the presence of RANKL (100 ng/mL) and were able to notice a potent inhibitory effect of eupatilin on osteoclastogenesis; complete absence of TRAP + OC was seen at 50 μM eupatilin (***$P < 0.001$) (Fig. 1A). When using BMCs, no or marginal cytotoxic effect was associated with eupatilin by detecting the absorbance optical density from XTT assay based on the medium (Fig. 1B). Formation of OB remained unaffected at 25 μM or significantly downregulated at 50 μM based upon ALP activity (***$P < 0.001$) (Fig. 1C), suggesting that eupatilin may preferentially act on OCs and show cytotoxicity on OB at 50 μM. Eupatilin completely blocked F-actin formation (Fig. 1D), suggesting that eupatilin, at least, affects cytoskeleton rearrangement. Real-time RT-PCR experiments showed that *c-Fos* and *NFATc1* mRNAs were significantly downregulated in a time-dependent manner and no *TRAP* mRNA was detected, confirming the TRAP staining results. (*$P < 0.05$, **$P < 0.01$, and ***$P < 0.001$) (Fig. 2A–C). Complete suppression of *OSCAR*, *OC-STAMP* and *cathepsin K* transcription was achieved (**$P < 0.01$, and ***$P < 0.001$) (Fig. 2D–F) and transcription of *DC-STAMP*, *Integrin β3*, *Integrin αv* and *ICAM-1*

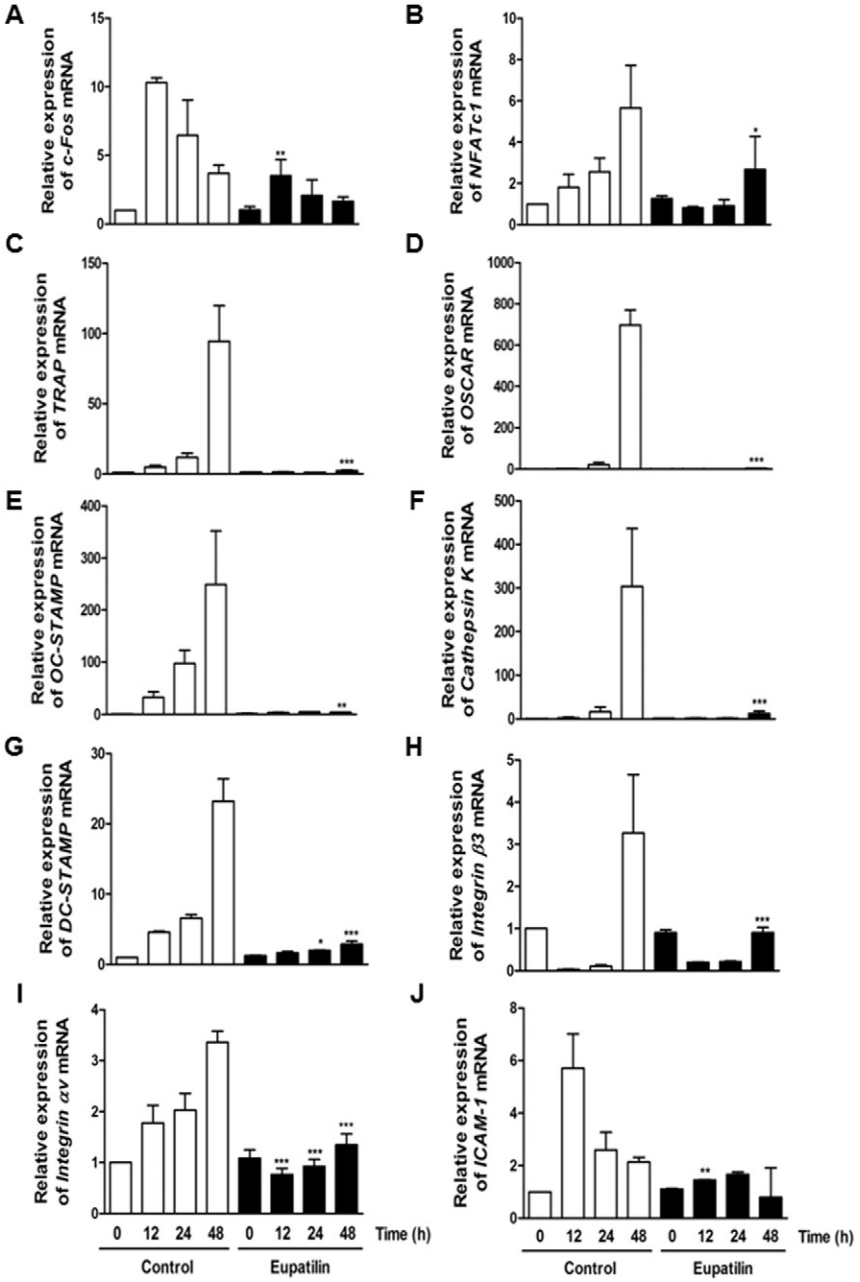

Fig. 2. Effects of eupatilin on downregulation of OC-specific genes involved in transcription repression of NFATC1 and differentiation of OC. BMMs were pre-treated with or without eupatilin (50 μM) for 1 h and with RANKL (100 ng/mL) for the indicated times. Expression of *c-Fos*, *NFATc1*, *TRAP* (A–C), *OSCAR*, *OC-STAMP*, *cathepsin K* (D–F), *DC-STAMP*, *Integrin β3* and *αv* (G–I), and *ICAM-1* (J) mRNA level was analyzed real-time RT-PCR.

was substantially blocked ($^{*}P < 0.05$, $^{**}P < 0.01$, and $^{***}P < 0.001$) (Fig. 2G–J). This may indicate that elimination of *cathepsin K* transcription by eupatilin has an inhibitory ability on bone resorption associated with eupatilin. The phosphorylation status of several early signal transducers was examined upon eupatilin stimulation. Eupatilin markedly inhibited phosphorylation of Akt, GSK3β, IκB (Fig. 3A–B) and to a lesser extent blocked that of ERK at 30 min after stimulation (Fig. 3C) whereas neither p38 nor JNK was affected by eupatilin. This suggests that these kinases may not be linked to activity of eupatilin in terms of anti-osteoclastogenesis (Fig. 3C). It should be noted that c-Fos and NFATc1 protein levels were substantially reduced (Fig. 3D). To substantiate these inhibitory mechanisms restoration experiments were performed. In vitro osteoclastogenesis assays were conducted with the use of overexpression of constitutively active or wild type transcription factors in the presence of 25 μM eupatilin. No TRAP+ MNCs were recovered even after overexpression of transcription factors. While overexpression of constitutive *c-Fos* or *NFATc1* demonstrated a significant restoration ($^{\#}P < 0.05$, $^{\#\#}P < 0.01$, and $^{***}P < 0.001$) (Fig. 4A–B) only a partial restoration of TRAP+ MNCs resulted from overexpressing constitutive active IκB and Akt ($^{*}P < 0.05$ and $^{***}P < 0.001$) (Fig. 4C-D). In particular, overexpression of constitutive *NFATc1* restore MNCs to a greater extent than other genes overexpressed. One of the major signaling read-outs elicited by RANKL is NF-κB activation, contributing to induction of the transcription of *NFATc1*. To see whether eupatilin inhibits NF-κB activation, a ligand-dependent reporter assay was conducted as seen in Fig. 4E ($^{\#\#\#}P < 0.001$ and $^{***}P < 0.001$) Eupatilin was able to significantly attenuate luciferase activities in both a ligand-dependent and dose-dependent manner, strongly suggesting that transcriptional repression of NF-κB is a way by which eupatilin blocks osteoclastogenesis, presumably culminating in induction of NFATc1. Taken together, these data suggest that eupatilin effectively blocks osteoclastogenesis via rapidly blunting phosphorylation of Akt, GSK3β, ERK or NF-κB, resulting in downregulation of NFATc1.

3.2. Eupatilin is a potent inhibitor of actin polymerization of MNCs

Since eupatiln was able to significantly attenuate *cathepsin K* transcription and dismantle F-actin formation, we hypothesized that eupatilin could also block bone-resorption capability of MNCs. MNCs were cultured on hydroxyapatitite or dentin scaffold in the presence of varying concentrations of eupatilin for 24 h. Pit formation and bone resorbed area were enumerated. As shown in Fig. 5A–B, treatment of these MNCs with 25 μM or 50 μM eupatilin completely eliminated pit formation and bone-resorption capability associated with MNCs ($^{**}P < 0.01$, and $^{***}P < 0.001$). We initially noticed that those eupatilin-treated MNCs on dentins underwent substantial morphological change by deforming cell membrane into an irregular shape. This may raise the question that the strong blockade of bone resorption by eupatilin is not due to cathepsin K, since complete transcriptional suppression of *cathepsin K* occurred as shown in the earlier real-time RT-PCR experiments. However, fully functional MNCs were situated at the dentin surface, and exocytosis of *cathepsin K* might have taken place. Hence, actin polymerization might be a key milestone linked to eupatilin-mediated inhibition of bone resorption. We further determined whether eupatilin can dismantle actin ring structure/formation by visualizing phallodin probe. Confocal imaging analysis suggests that treatment with eupatilin completely dismantled actin ring as shown in Fig. 5C. Since DAPI staining remained intact it appears that eupatilin may not cause apoptosis. Since the duration of complete inhibition of the bone resorption took placed within 24 h we asked whether pre-treatment of mouse BMMs with eupatilin would lead to inhibition of differentiation of OC. As shown in Fig. 5D, eupatilin pre-treatment for only 3 h caused a substantial attenuation of generation of TRAP+ OC and TRAP+ MNCs. At 6 h near complete inhibition was noted, suggesting that a brief exposure of BMMs to eupatilin gives rise to a momentum responsible for blocking commitment of macrophages to OC and further to MNCs via engagement of RANK with RANKL ($^{*}P < 0.05$ $^{***}P < 0.001$).

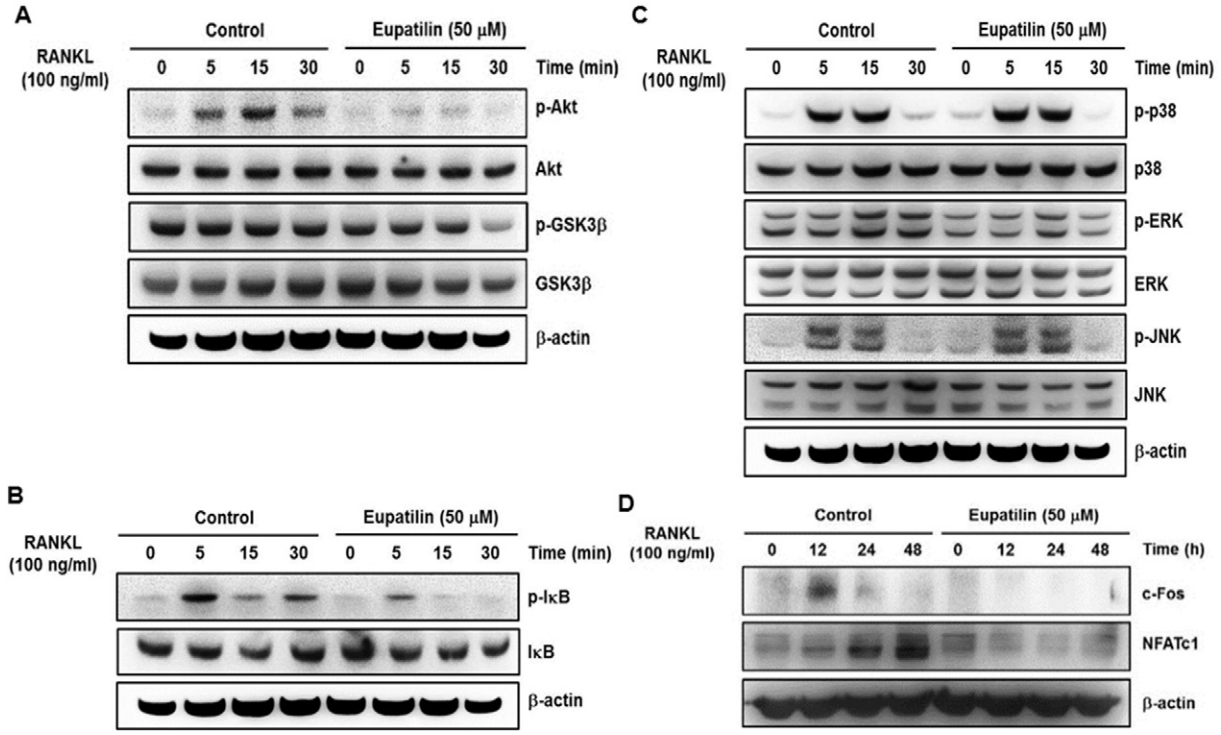

Fig. 3. Effects of eupatilin on phosphorylation of kinases or transcription factors, and on decreases in c-Fos and NFATc1. Mouse BMCs were pre-treated with the eupatilin (50 μM) or control for 1 h in the presence of M-CSF (30 ng/mL) and were then stimulated with RANKL (100 ng/mL) for the indicated time points. Whole-cell lysates were subjected to Western blot analysis with the indicated antibodies. (A–C) phosphorylation of Akt, GSK3β, IκB, ERK, respectively, and (D) attenuated protein levels of c-Fos and NFATc1.

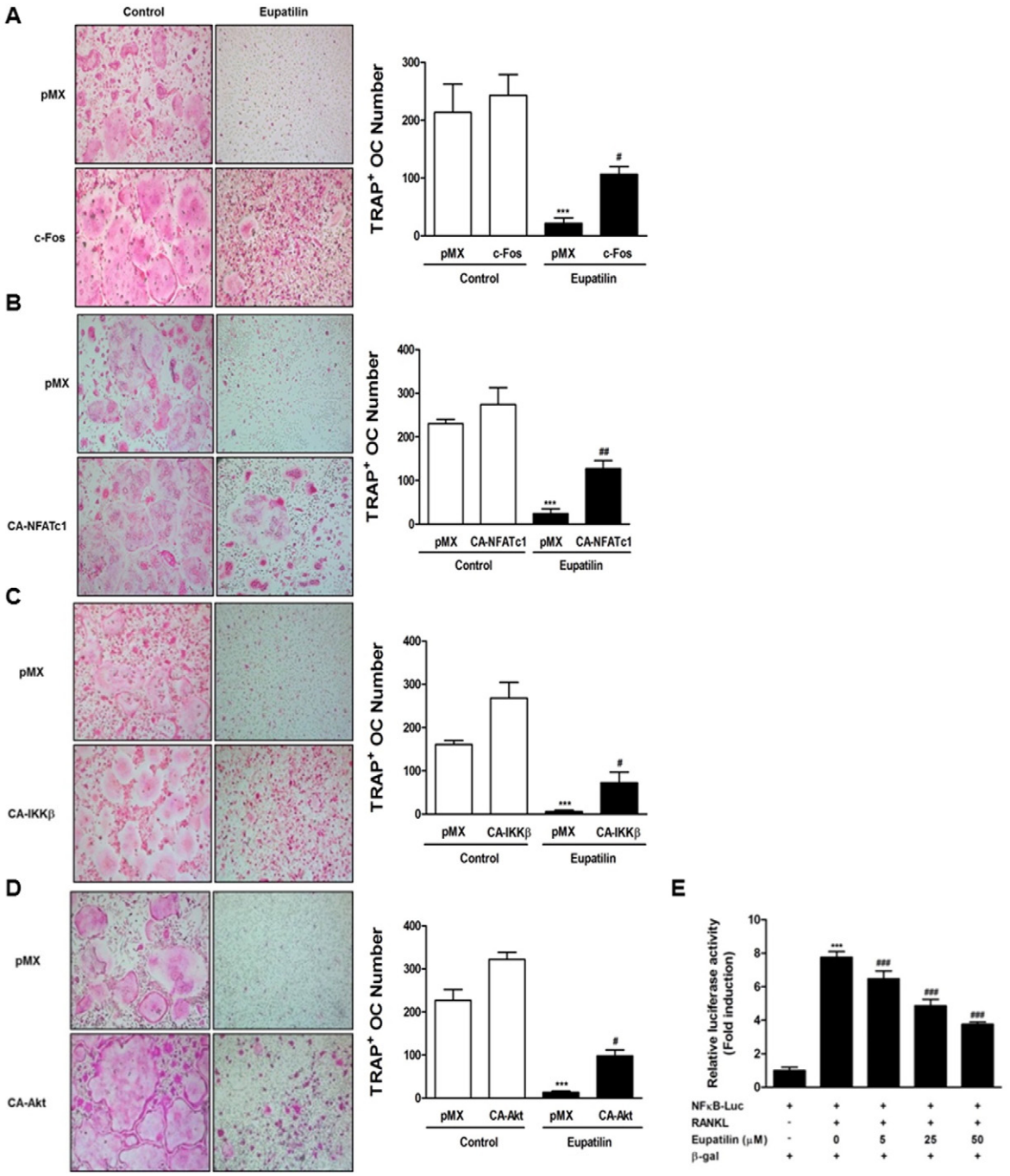

Fig. 4. Restoration of osteoclastogenic potential via overexpression. (A–B) Mouse BMMs were infected with retroviruses bearing *c-Fos*, a constitutively active form of *NFATc1* or vehicle. Infected BMMs were cultured with or without eupatilin (25 μM) in the presence of M-CSF (30 ng/mL) and RANKL (100 ng/mL) for 4 days. TRAP-positive multinucleated osteoclasts were counted. (C–D) Mouse BMMs were infected with retroviruses bearing a constitutively active form of IκB, a catalytically active Akt or vehicle. Differentiation and TRAP staining was conducted as described above. The magnification of images is 10×. (E) Mouse RANK-expressing 293T cells were transfected with NF-κB-driven luciferase and stimulated with RANKL (100 ng/mL) or control in the increasing concentrations of eupatilin. Luciferase activities were normalized by those of β-gal.

We further asked whether eupatilin could affect MNCs during or after differentiation. Normally, fully differenced MNCs appear at 72 h upon *RANKL* treatment. Indeed, at 24 h prior to complete differentiation, during which time MNCs were being generated, eupatilin-treated MNCs exhibited a significant reduction of cytoplasm and accumulation of fused nuclei as denoted by arrow bars in Fig. 5E. Observation under high magnification power clearly showed that a vast majority of 24 h-long eupatilin-treated TRAP + OC or MNCs shrank and yielded fibroblast-like appendages. Control TRAP + OC was clustered, possibly due to directed cell migration for cell fusion. Control MNCs or 6 h eupatilin-treated MNCs contain a large cytoplasm containing distributive multiple nuclei. Taken together, these bone resorption assays and imaging analysis suggests that eupatilin effectively induces cell shape change, probably via actin depolymerization.

3.3. Effect of eupatilin on phosphorylation of cofilin and expression of TESK1 and LIMK2

To see if eupatilin modulates actin polymerization, phosphorylation of cofilin was checked. As shown in Fig. 6A, eupatilin significantly attenuated phosphorylation of cofilin but phosphorylated cofilin was sustained until 48 h after stimulation with RANKL, suggesting that

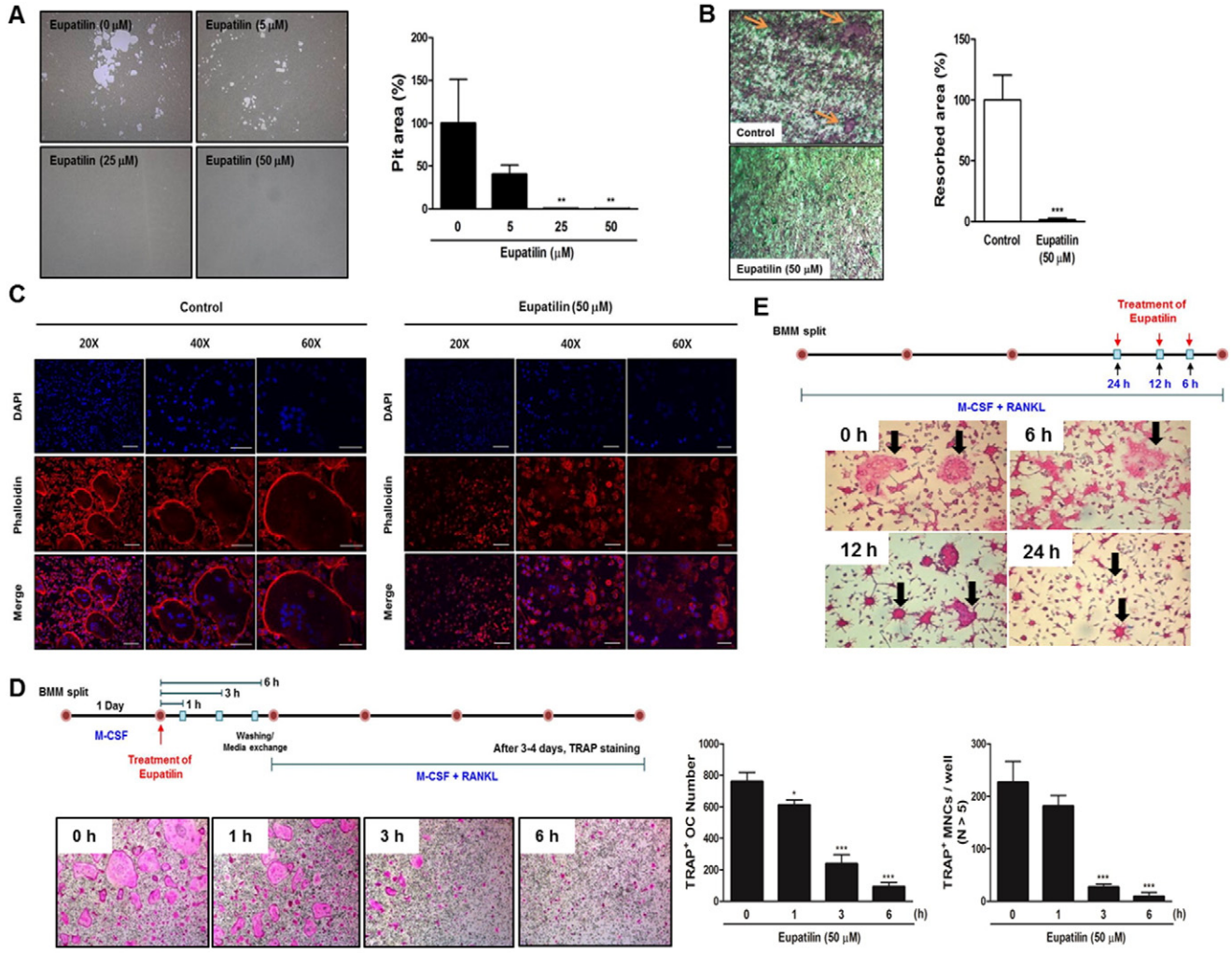

Fig. 5. Effects of eupatilin on bone resorption and cell shape change. (A) MNCs were seeded on hydroxyapatite-coated plates and treated with the indicated concentrations of eupatilin for 24 h or 48 h. Pit areas were quantified using ImageJ (right). The magnification of images is 10×. (B) MNCs were cultured on dentin slices and treated with eupatilin (50 μM). Resorbed areas were stained and measured. The magnification of images is 10×. (C) Mouse BMCs were cultured for 4 days in the presence of M-CSF (30 ng/mL) and RANKL (100 ng/mL) on glass coverslip and treated with control or eupatilin (50 μM). Cells were fixed and stained with rhodamine phalloidin to detect actin ring. Images in the bottom of panels were merged with the images of upper panels including phalloidin and DAPI staining. (D) After stimulating BMMs with M-CSF (30 ng/mL), overnight BMMs were pre-treated with eupatilin (50 μM) for 1 h, 3 h or 6 h followed by washing the stimulated cells. Cells were then stimulated with M-CSF (30 ng/mL) and RANKL (100 ng/mL) for 3 days and stained with TRAP solution. TRAP-positive OC and MNCs were counted. The magnification of images is 10×. (E) Mouse BMCs were differentiated into mature OC for 3 days, treated with eupatilin for 6 h, 12 h, or 24 h prior to complete differentiation and stained with TRAP solution. The magnification of images is 10×. Normal or deformed MNCs are indicated with arrow bars.

cofilin may not be a major target for eupatilin in OC. We investigated whether eupatilin may regulate two kinases, *TESK1* and *LIMK2*. As shown in Fig. 6B–C, basal levels *TESK1* and *LIMK2* were sharply downregulated 12 h after RANKL treatment and remained constant at these basal levels thereafter. 1 h pre-treatment of BMMs with eupatilin further diminished basal levels of *TESK1* or *LIMK2* (which is denoted by arrows) (***$P < 0.001$). Another set of real-time PCR experiment revealed that mRNA levels of these kinases rapidly dropped to basal levels within 2 h after stimulation with RANKL (data not shown), suggesting that downregulation of these kinases play some role in osteoclasotogenesis within the natural RANKL/RANK axis. Hence, correlation of functions of these kinases to eupatilin is obscure and how these kinases work on osteoclastgenesis in a concerted manner with *RANK* downstream remains to be determined.

3.4. Eupatilin exhibits a potent inhibitory effect on differentiation of human OC

To see if eupatilin was also able to block human osteoclastogenesis, in vitro assays were performed using human OC. As shown in Fig. 7, a dose-dependent inhibition of generation of TRAP+ human OC was revealed in the presence of M-CSF (30 ng/mL) and RANKL (100 ng/mL), suggesting that eupatilin treatment may be useful for the treatment of human osteoporosis (***$P < 0.001$).

3.5. Potent therapeutic capabilities associated with oral administration of eupatilin for bone regeneration in two murine osteoporotic models

The two distinct activities associated with eupatilin, namely transcriptional suppression and inhibition of actin rearrangement, prompted us to test whether eupatilin could effectively reduce bone resorption in two different mouse models; 1) LPS-induced bone loss (Negishi-Koga et al., 2011) and 2) OVX-induced bone loss (Koga et al., 2004). Each model has two different sub-models to validate effectiveness of eupatilin on bone loss as seen in Figs. 8 and 9. A normal LPS model was conducted as shown in Fig. 8A. Eupailin per se did not generate an overt harmful effect on control mice. Examination of other organs has been not assessed.

For a therapeutic model, LPS was administered intra-peritoneally into mouse at day 0. Significant bone loss was noted at day 5, inferring

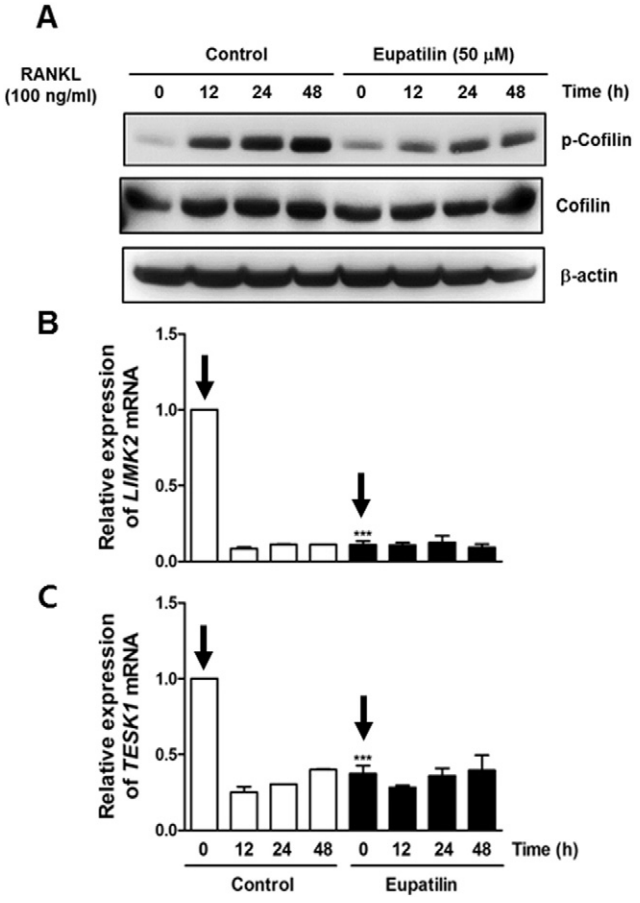

Fig. 6. Dephosphorylation of cofilin and rapid downregulation of TESK1 and LIMK2 in response to eupatilin. (A) Cell lysates were prepared in the presence or absence of eupatilin. Western blot analysis was performed with a phosphor-specific cofilin, total cofilin, or β-actin antibody. (B–C) Mouse BMMs were pre-treated with eupatilin (50 μM) or control for 1 h and differentiation was driven by addition of RANKL (100 ng/mL) for the indicated time points. mRNAs were then extracted and expression of *TESK1* and *LIMK2* mRNA levels were analyzed with real-time RT-PCR. The mRNA levels at time zero, namely 1 h after eupatilin or control pre-treatment, were indicated with arrows for comparison.

that bone loss would have begun earlier. LPS was administered at day 4 followed by oral delivery of eupatilin 3 times at days 4, 6 or 8 in which each delivery was accompanied by boost injection at every two days till 10 days when fulminant bone loss was evident as shown Fig. 8D–E. Surprisingly, eupatilin completely prevented bone loss in each model ($^{*}P < 0.05$, $^{**}P < 0.01$, $^{***}P < 0.001$, $^{\#}P < 0.05$, $^{\#\#}P < 0.01$, and $^{\#\#\#}P < 0.001$) (Fig. 8C–F). Especially, it should be noted that only double oral administrations of eupatilin at day 8 was capable of healing LPS-induced bone loss in the therapeutic model as evident by the effects of eupatilin on bone-related parameters that up-regulation of bone volume and downregulation of trabecular bone separation ($^{**}P < 0.01$, $^{***}P < 0.001$, $^{\#}P < 0.05$, $^{\#\#}P < 0.01$, and $^{\#\#\#}P < 0.001$) (Fig. 3F). Two OVX-induced bone loss models were designed such that while the normal therapeutic model took 4 weeks for induction of osteoporosis, an aggressive therapeutic model took an extended 8 weeks for induction of osteoporosis followed by 4 weeks treatment (Fig. 9A and D). The aggressive model exhibited more significant bone loss than the normal model as shown in Fig. 9B and E. Eupatilin-treated OVX mice exhibited a significant restoration of bone loss as compared with sham controls from these two models ($^{*}P < 0.05$, $^{**}P < 0.01$, $^{***}P < 0.001$, and $^{\#}P < 0.05$) (Fig. 9C and F). Increase in bone volume and tibia number is especially notable.

4. Discussion

We observed that pre-treatment, post-treatment, or any interim treatments of OCs with eupatilin greatly affected the biological status of OCs. This suggests that eupatilin gives rise to multifaceted effects on OCs. Transcriptional suppression of *c-Fos* or *NFATc1* by eupatilin may be restricted to OCs existing at very early differentiation stages, because eupatilin was able to inhibit phosphorylation of Akt, GSK3β, ERK and IκB within 30 min. In osteoclastogenesis, several early signaling including Akt, GSK3β, NF-κB and ERK are reported to be required for optimal induction of NFATc1 (Feng et al., 2014). Also, it has been reported that attenuation of calcium immobilization or inhibition of NF-κB or ERK in part accounts for flavonoid-mediated anti-osteoclastogenesis (Yamaguchi et al., 2007; Ang et al., 2011). Although we did not perform calcium oscillation with the treatment of eupatilin to BMMs our data are

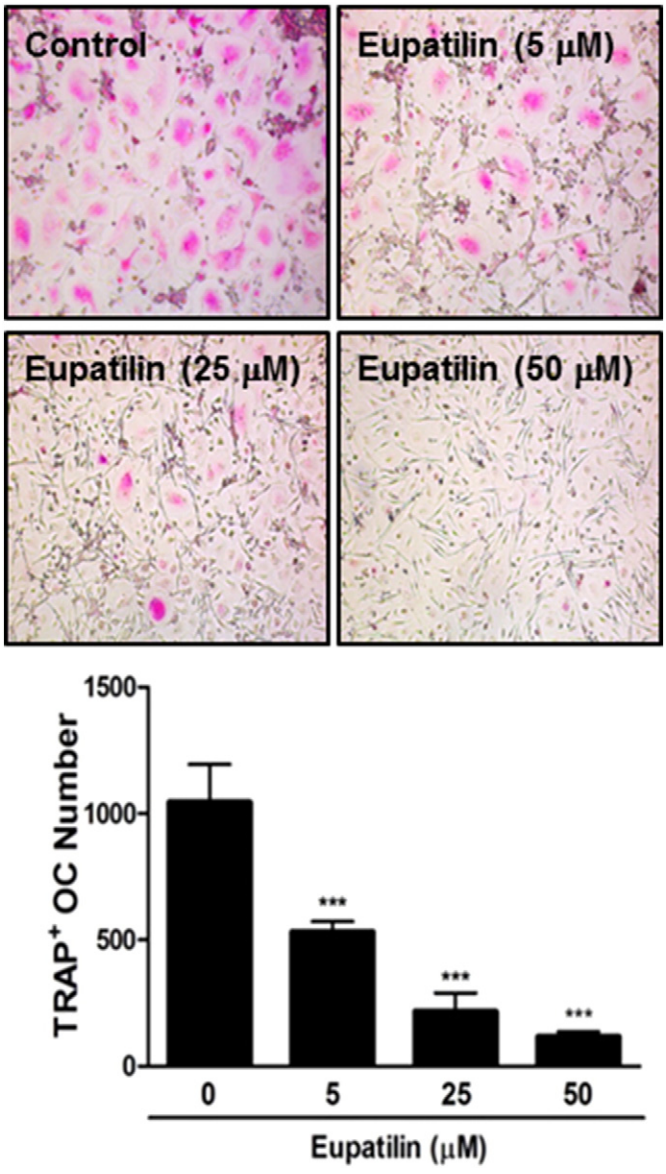

Fig. 7. Potent inhibition of human osteoclastogenesis by eupatilin in vitro. Human BMCs were obtained from voluntary donors and differentiated with M-CSF (30 ng/mL) and RANKL (100 ng/mL) for 9 days with a change of same conditioned medium every 3 days. Then, human TRAP-positive osteoclasts were subjected to TRAP assay in the presence of increasing concentrations of eupatilin or vehicle. TRAP+ human OC (nuclei > 3) were enumerated by microscopic observation. The magnification of images is 10×.

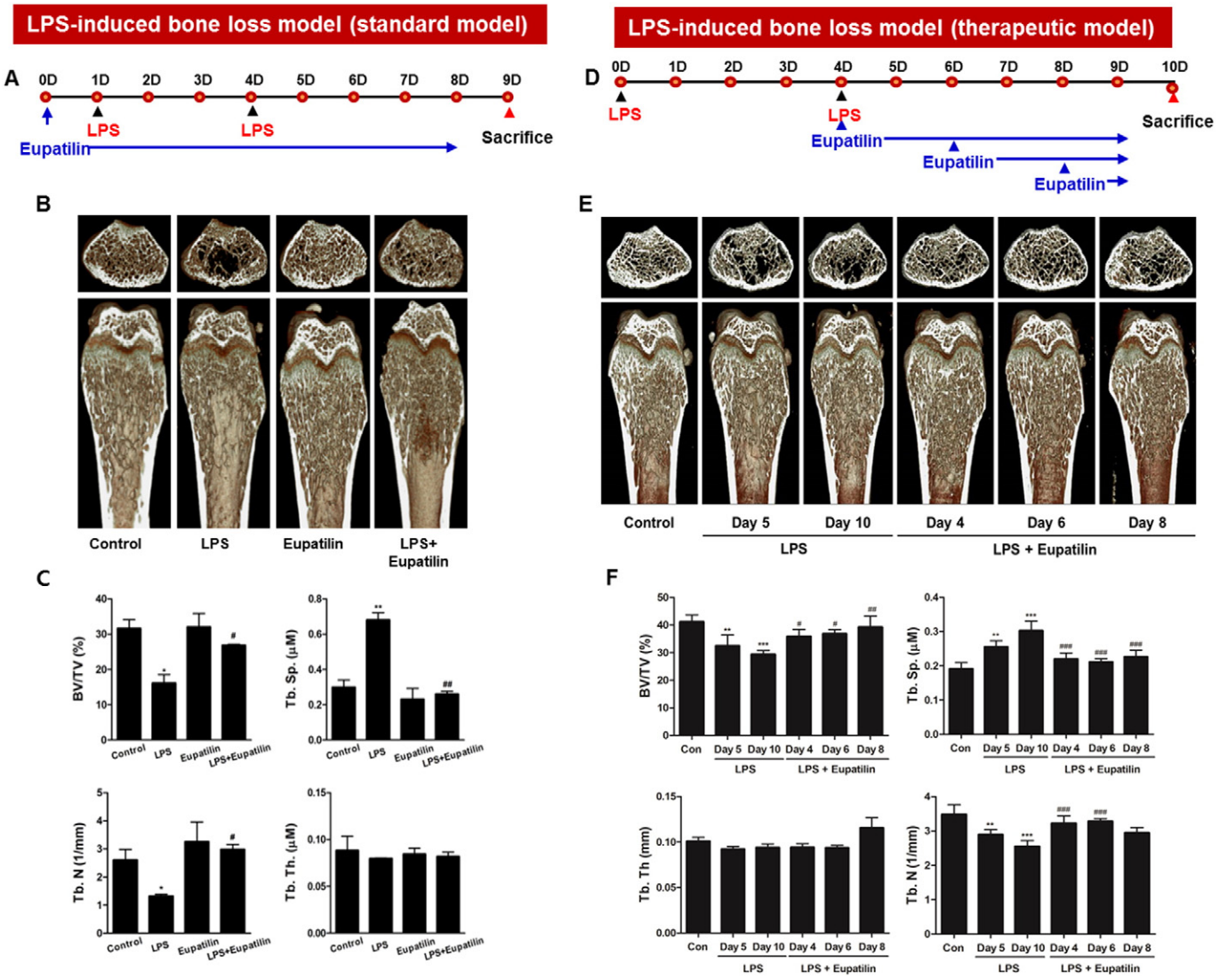

Fig. 8. Complete regeneration of LPS-induced bone loss by eupatilin. (A) Two different strategies of bone loss induction and oral administration are shown. (B) Normal model; 5 mice or control mice were administered eupatilin 1 day prior to the 1st LPS injection (5 mg/kg) represented by day 0. The 2nd LPS injection (5 mg/kg) was conducted on day 2 followed by daily oral delivery of eupatilin until killed at day 8. Radiographs of the longitudinal and transverse section of the proximal femurs were obtained with a μ-CT apparatus. (C) The trabecular bone volume/total volume (BV/TV), trabecular separation (Tb·Sp), trabecular thickness (Tb·Th), and trabecular number (Tb·N) of the femurs were determined using the μ-CT data as analyzed with INFINITT-Xelis software. $^{**}P < 0.01$ and $^{***}P < 0.001$ versus the control group, and $^{\#}P < 0.05$, $^{\#\#}P < 0.01$, and $^{\#\#\#}P < 0.001$ versus the LPS group. Each experiment was performed once but some time points were conducted twice for verification. (D) Therapeutic model; LPS (5 mg/kg) was injected at day 0 and day 4. Eupatilin was administered at day 4, day 6 or day 8 followed by daily delivery until killed. (E) The same CT was performed and analyzed as described in (B). (F) The same parameters were used for bone regeneration as described in (C).

consistent with inhibition of NF-κB or ERK upon RANK activation. Our RANKL-dependent transient activation of NF-κB and overexpression following restoration data clearly suggests that eupatilin is a potent inhibitor of induction of c-Fos or NFATc1. Although we do not delineate the inhibition of such rapid phosphorylation of these kinases or IκB via eupatilin it is likely that eupatilin might affect lipid kinases such as PI3K and PDK or Ras signaling pathway. Regarding inhibition of *c-Fos* as an immediate early gene, immediate early signal transducers such as serum response factor SRF involving SAP-1 or Elk1 might be targets for eupatilin as well (Dalton and Treisman, 1992; Miranti et al., 1995). Action modes of rapid transcriptional repression of *c-Fos* or *NFATc1* by eupatilin remains to be further delineated.

Along with this transcription repression model, we observed that contacting effect of eupatilin on OCs was prominent. Pre-treatment of mouse BMMs with 50 μM eupatilin for only 3 h gave rise to dramatic inhibition of OC differentiation or formation of MNCs. Even interim-treatment or post-treatment strikingly affected cell fusion as well as morphological changes, and eupatilin completely blocked pit formation. The rhodamine–phalloidin imaging feature strongly suggests that cytoskeletal rearrangement of OCs induced by eupatilin may be an important mechanism through which formation of MNCs is affected, as cells became morphologically transformed into fibroblast-like cells. While this manuscript was in preparation, Li et al. reported that naringin, a flavonoid, induced apoptosis of OCs via mitochondrial dismantling (Li et al., 2014). However, we did see intact nuclei via DAPI whereas actin ring was markedly prevented from forming. Both inhibition of F-actin formation and bone resorption, and phosphorylation of cofilin by eupatilin strongly indicate that another major action mode is a cytoskeletal change through alteration of actin. Previously, it was reported that TESK1 and LIMK2 play a pivotal role in reprogramming mouse embryonic fibroblasts into embryonic stem cells via phosphorylation of cofilin which is responsible for actin polymerization (Sakurai et al., 2014). Since eupatilin treatment was unable to shut down sustained phosphorylation of cofilin until 48 h we believe that there could be an OC-specific contributing factor(s) to actin depolymerization specifically-targeted by eupatilin. Since it has been shown that cytoskeletal change is coupled to transcription (Miralles et al., 2003), the cytoskeletal change induced by eupatilin

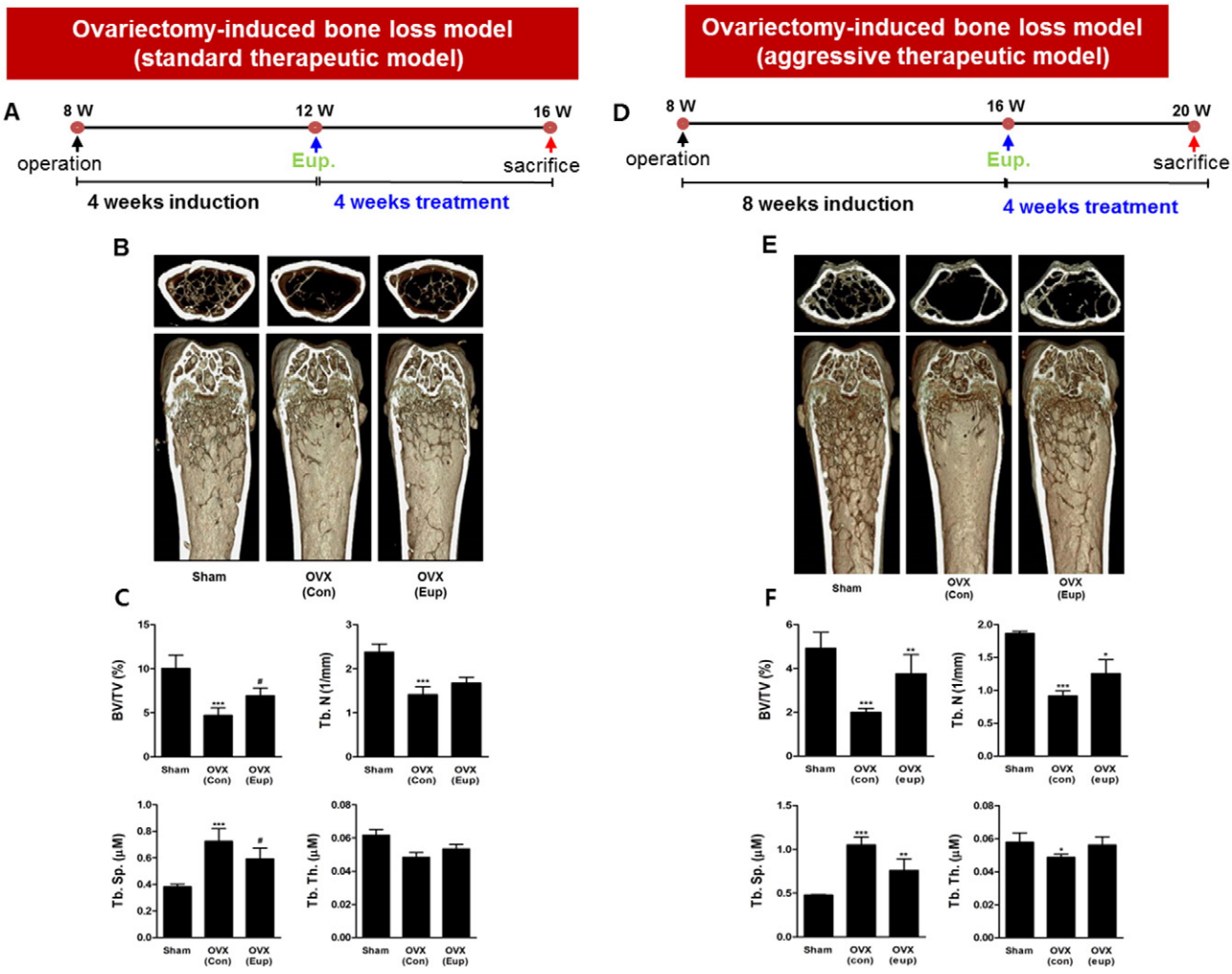

Fig. 9. Significant amelioration of OVX-mediated osteoporosis by eupatilin. (A) Scheme for normal disease induction and treatment. (B) Normal model; 5 OVX mice or 5 SHAM control mice subjected to initiation of osteoporosis for 4 weeks from ovariectomy followed by oral administration of eupatilin for another 4 weeks. Radiographs of longitudinal and transverse sections of the proximal femur of OVX mice were obtained with a μ-CT apparatus (upper). (C) Similar parameters were used for measuring bone regeneration as described in the LPS-induced bone loss model. (D) Aggressive model; 5 OVX mice or 5 SHAM control mice subjected to initiation of osteoporosis for 8 weeks from ovariectomy followed by oral administration of eupatilin for another 4 weeks. E–F) The same measurement for bone regeneration was applied to this aggressive model. Each experiment was performed once. Their statistics were measured with INFINITT-Xelis software. $^{**}P < 0.01$ and $^{***}P < 0.001$ versus SHAM group, and $^{\#}P < 0.05$, $^{\#\#}P < 0.01$, and $^{\#\#\#}P < 0.001$ versus the OVX group.

could be linked to transcription, thereby modulating differentiation of OCs. We believe that cytoskeletal rearrangement coupled to transcriptional repression may be the most plausible mechanism for the eupatilin-mediated anti-osteoclastogenesis. With respect to cell toxicity, eupatilin exhibited no influence on viability of bone marrow cells or a marginal effect on osteoblastogenesis at 50 μM, which is the highest concentration in our preparation, suggesting that OCs might be a preferential natural target for eupatilin over OB. Our observation that control mice given oral administration of eupatilin (10 mg/kg) appeared healthy also suggests that cell toxicity is not associated with eupatilin. *Artemisia* herb extracts have been safely used for many inflammatory diseases like gastritis or malaria over a few thousand years (Li and Wu, 1998). Osteoporosis is an aging-associated disease. And it is also becoming clear that OCs are believed to be a major player in tumor bone metastasis (Jones et al., 2006). Osteolysis by metastasized tumor still requires new therapeutic interventions (Morony et al., 2001). OCs have been well appreciated to play a pivotal role in bone deformation acquired by rheumatoid arthritis. Gingivitis is a common disease to adults, which is associated with inflammation-driven differentiation of OCs (Terheyden et al., 2014). Two outstanding therapeutic features associated with eupatilin are 1) preferential target-specificity, namely OCs and 2) robustness of elimination of pathogenic MNCs through immediate cessation of cytoskeletal change and transcription, leading to actin depolymerization and disintegration of MNCs. Taken together, eupatilin could provide a good opportunity permitting a versatile therapeutic modality for a broad range of bone diseases to be developed, as supported by our finding that human OCs are affected by eupatilin in vitro. Also, further study is needed to confirm the in vitro effects of eupatilin on LPS-induced inflammatory osteoclast differentiation.

Acknowledgments

This study was supported by an intramural fund from OsteoNeuroGen (ONG100PA1) and a grant from the Korean Health Technology R&D Project, Ministry of Health & Welfare, and Republic of Korea (HI12C0110). The use of experimental animals was reviewed by the IACUC and was approved under WKU14-17. All human subjects were reviewed and approved by WK IRB under WKUH-HRBR-032. We are deeply indebted to Dr. Hal E Broxmeyer for valuable comments and proofreading of this manuscript.

References

Ang, E.S., Yang, X., Chen, H., Liu, Q., Zheng, M.H., Xu, J., 2011. Naringin abrogates osteoclastogenesis and bone resorption via the inhibition of RANKL-induced NF-kappaB and ERK activation. FEBS Lett. 585, 2755–2762.

Cha, J.D., Moon, S.E., Kim, H.Y., Cha, I.H., Lee, K.Y., 2009. Essential oil of *Artemisia capillaris* induces apoptosis in KB cells via mitochondrial stress and caspase activation mediated by MAPK-stimulated signaling pathway. J. Food Sci. 74, T75–T81.

Choi, E.J., Lee, S., Chae, J.R., Lee, H.S., Jun, C.D., Kim, S.H., 2011. Eupatilin inhibits lipopolysaccharide-induced expression of inflammatory mediators in macrophages. Life Sci. 88, 1121–1126.

Dalton, S., Treisman, R., 1992. Characterization of SAP-1, a protein recruited by serum response factor to the c-fos serum response element. Cell 68, 597–612.

Feng, W., Xia, W., Ye, Q., Wu, W., 2014. Osteoclastogenesis and osteoimmunology. Front. Biosci. 19, 758–767.

Geusens, P., Chapurlat, R., Schett, G., Ghasem-Zadeh, A., Seeman, E., de Jong, J., et al., 2014. High-resolution in vivo imaging of bone and joints: a window to microarchitecture. Nat. Rev. Rheumatol. 10, 304–313.

Ho, W.E., Peh, H.Y., Chan, T.K., Wong, W.S., 2014. Artemisinins: pharmacological actions beyond anti-malarial. Pharmacol. Ther. 142, 126–139.

Honma, M., Ikebuchi, Y., Kariya, Y., Suzuki, H., 2014. Regulatory mechanisms of RANKL presentation to osteoclast precursors. Curr. Osteoporos. Rep. 12, 115–120.

Jeon, E.J., Lee, K.Y., Choi, N.S., Lee, M.H., Kim, H.N., Jin, Y.H., et al., 2006. Bone morphogenetic protein-2 stimulates Runx2 acetylation. J. Biol. Chem. 281, 16502–16511.

Ji, Y., Wang, L., Watts, D.C., Qiu, H., You, T., Deng, F., et al., 2014. Controlled-release naringin nanoscaffold for osteoporotic bone healing. Dent. Mater. 30, 1263–1273.

Jones, D.H., Nakashima, T., Sanchez, O.H., Kozieradzki, I., Komarova, S.V., Sarosi, I., et al., 2006. Regulation of cancer cell migration and bone metastasis by RANKL. Nature 440, 692–696.

Kim, J.Y., Cheon, Y.H., Oh, H.M., Rho, M.C., Erkhembaatar, M., Kim, M.S., et al., 2014a. Oleanolic acid acetate inhibits osteoclast differentiation by downregulating PLCgamma2-Ca(2+)-NFATc1 signaling, and suppresses bone loss in mice. Bone 60, 104–111.

Kim, J.Y., Cheon, Y.H., Oh, H.M., Rho, M.C., Erkhembaatar, M., Kim, M.S., et al., 2014b. Oleanolic acid acetate inhibits osteoclast differentiation by downregulating PLCγ2-Ca(2+)-NFATc1 signaling, suppresses bone loss in mice. Bone 60, 104–111.

Kim, Y.D., Choi, S.C., Oh, T.Y., Chun, J.S., Jun, C.D., 2009. Eupatilin inhibits T-cell activation by modulation of intracellular calcium flux and NF-kappaB and NF-AT activity. J. Cell. Biochem. 108, 225–236.

Kim, J.Y., Kim, J.Y., Cheon, Y.H., Kwak, S.C., Baek, J.M., Kim, Y.C., et al., 2014a. 9-Hydroxy-6,7-dimethoxydalbergiquinol inhibits osteoclast differentiation through down-regulation of Akt, c-Fos and NFATc1. Int. Immunopharmacol. 20, 213–220.

Kim, J., Kim, Y., Yi, H., Jung, H., Rim, Y.A., Park, N., et al., 2015. Eupatilin ameliorates collagen induced arthritis. J. Korean Med. Sci. 30, 233–239.

Kim, H.N., Lee, J.H., Bae, S.C., Ryoo, H.M., Kim, H.H., Ha, H., et al., 2011. Histone deacetylase inhibitor MS-275 stimulates bone formation in part by enhancing Dhx36-mediated TNAP transcription. J. Bone Miner. Res. 26, 2161–2173.

Koga, T., Inui, M., Inoue, K., Kim, S., Suematsu, A., Kobayashi, E., et al., 2004. Costimulatory signals mediated by the ITAM motif cooperate with RANKL for bone homeostasis. Nature 428, 758–763.

van der Kooy, F., Sullivan, S.E., 2013. The complexity of medicinal plants: the traditional *Artemisia annua* formulation, current status and future perspectives. J. Ethnopharmacol. 150, 1–13.

Kwak, H.B., Lee, B.K., Oh, J., Yeon, J.T., Choi, S.W., Cho, H.J., et al., 2010. Inhibition of osteoclast differentiation and bone resorption by rotenone, through down-regulation of RANKL-induced c-Fos and NFATc1 expression. Bone 46, 724–731.

Lee, C.H., Kwak, S.C., Kim, J.Y., Oh, H.M., Rho, M.C., Yoon, K.H., et al., 2014. Genipin inhibits RANKL-induced osteoclast differentiation through proteasome-mediated degradation of c-Fos protein and suppression of NF-kappaB activation. J. Pharmacol. Sci. 124, 344–353.

Li, Y., Wu, Y.L., 1998. How Chinese scientists discovered qinghaosu (artemisinin) and developed its derivatives? What are the future perspectives? Med. Trop. 58, 9–12.

Li, F., Sun, X., Ma, J., Ma, X., Zhao, B., Zhang, Y., et al., 2014. Naringin prevents ovariectomy-induced osteoporosis and promotes osteoclasts apoptosis through the mitochondria-mediated apoptosis pathway. Biochem. Biophys. Res. Commun. 452, 629–635.

Miralles, F., Posern, G., Zaromytidou, A.I., Treisman, R., 2003. Actin dynamics control SRF activity by regulation of its coactivator MAL. Cell 113, 329–342.

Miranti, C.K., Ginty, D.D., Huang, G., Chatila, T., Greenberg, M.E., 1995. Calcium activates serum response factor-dependent transcription by a ras- and elk-1-independent mechanism that involves a Ca^{2+}/calmodulin-dependent kinase. Mol. Cell. Biol. 15, 3672–3684.

Morony, S., Capparelli, C., Sarosi, I., Lacey, D.L., Dunstan, C.R., Kostenuik, P.J., 2001. Osteoprotegerin inhibits osteolysis and decreases skeletal tumor burden in syngeneic and nude mouse models of experimental bone metastasis. Cancer Res. 61, 4432–4436.

Negishi-Koga, T., Shinohara, M., Komatsu, N., Bito, H., Kodama, T., Friedel, R.H., et al., 2011. Suppression of bone formation by osteoclastic expression of semaphorin 4D. Nat. Med. 17, 1473–1480.

Sakurai, K., Talukdar, I., Patil, V.S., Dang, J., Li, Z., Chang, K.Y., et al., 2014. Kinome-wide functional analysis highlights the role of cytoskeletal remodeling in somatic cell reprogramming. Cell Stem Cell 14, 523–534.

Semënov, M., Tamai, K., He, X., 2005. SOST is a ligand for LRP5/LRP6 and a Wnt signaling inhibitor. J. Biol. Chem. 280, 26770–26775.

Son, J.E., Lee, E., Seo, S.G., Lee, J., Kim, J.E., Kim, J., et al., 2013. Eupatilin, a major flavonoid of *Artemisia*, attenuates aortic smooth muscle cell proliferation and migration by inhibiting PI3K, MKK3/6, and MKK4 activities. Planta Med. 79, 1009–1016.

Suda, T., Takahashi, N., Udagawa, N., Jimi, E., Gillespie, M.T., Martin, T.J., 1999. Modulation of osteoclast differentiation and function by the new members of the tumor necrosis factor receptor and ligand families. Endocr. Rev. 20, 345–357.

Takayanagi, H., Kim, S., Matsuo, K., Suzuki, H., Suzuki, T., Sato, K., et al., 2002. RANKL maintains bone homeostasis through c-Fos-dependent induction of interferon-beta. Nature 416, 744–749.

Terheyden, H., Stadlinger, B., Sanz, M., Garbe, A.I., Meyle, J., 2014. Inflammatory reaction — communication of cells. Clin. Oral Implants Res. 25, 399–407.

Williamson, E., Bilsborough, J.M., Viney, J.L., 2002. Regulation of mucosal dendritic cell function by receptor activator of NF-kappa B (RANK)/RANK ligand interactions: impact on tolerance induction. J. Immunol. 169, 3606–3612.

Yamaguchi, M., Hamamoto, R., Uchiyama, S., Ishiyama, K., 2007. Effects of flavonoid on calcium content in femoral tissue culture and parathyroid hormone-stimulated osteoclastogenesis in bone marrow culture in vitro. Mol. Cell. Biochem. 303, 83–88.